Sensors and Materials, Vol. 37, No. 7 (2025) 2949–2970
MYU Tokyo

S & M 4096

Effective Wind Power Fluctuation Diminishment Using Improved Complete Ensemble Empirical Mode Decomposition with Adaptive Noise and Hilbert Spectral Analysis in Hybrid Energy Storage Systems

Muhammad Nouman Shahzad,[1,2] Obaid ur Rahman,[1,2] Hsiung-Cheng Lin,[3*] Asif Hussain,[4] and Ling-Ling Li[1,2]

[1]Key Laboratory of Electromagnetic Field and Electrical Apparatus Reliability of Hebei Province, Hebei University of Technology, Tianjin 300401, China
[2]State Key Laboratory of Intelligent Power Distribution Equipment and System, Hebei University of Technology, Tianjin 300401, China
[3]Department of Electronic Engineering, National Chin-Yi University of Technology, Taichung 41170, Taiwan.
[4]Department of Physics, The University of Lahore 54000, Lahore, Pakistan

(Received April 24, 2025; accepted June 17, 2025)

Keywords: smoothing wind power fluctuation, improved complete ensemble empirical mode decomposition with adaptive noise, hybrid energy storage system, Hilbert transform, power sharing

The integration of large-scale wind power into modern grids gives rise to a complicated issue due to meteorological variability, threatening power stability and security. Although these adverse effects can be somehow mitigated by leveraging the geo-spatiotemporal distribution through the rapid response of energy storage devices, the wind power fluctuations are being increasingly taken up in public debate, even influencing energy prices and leading to acceptance problems. For this reason, in this work, we aim to minimize wind power fluctuations using improved complete ensemble empirical mode decomposition with adaptive noise (ICEEMDAN) and Hilbert spectral analysis in a hybrid energy storage system (HESS). Initially, *K*-means clustering is used to find cluster center positions. Each cluster, median fluctuations, and noise levels are then analyzed from typical daily data. Statistical analysis to smooth wind output power is conducted, incorporating a weighted combination of moving average filtering (MAF) and anti-pulse interference average filtering (AIAF) algorithms. The HESS reference power is decomposed into various intrinsic mode functions (IMFs) spanning high- to low-frequency bands using ICEEMDAN methods. The time–frequency characteristics of each IMF are derived using Hilbert transform (HT) analysis. High-frequency power fluctuations are managed by a supercapacitor, whereas the battery handles low-frequency components. The effectiveness of the proposed strategy is validated using actual sampling data, demonstrating that the impact of wind power fluctuations on grid stability can be significantly reduced.

*Corresponding author: e-mail: hclin@ncut.edu.tw
https://doi.org/10.18494/SAM5708

ISSN 0914-4935
https://myukk.org/

1. Introduction

As global climate change intensifies, decarbonization has become an urgent priority worldwide. Among renewable energy options, wind power has gained prominence owing to its clean energy generation and pivotal role in advancing sustainable power systems. Its abundant availability and ecofriendly attributes make wind power a pivotal element in efforts to mitigate climate change and energy sustainability. Consequently, optimizing wind energy utilization is essential for enhancing its contribution to a cleaner, more resilient energy landscape.(1) On the other hand, energy storage batteries are essential for the temporal and spatial translation of electric energy, as they help to smooth fluctuations in wind power output. However, relying on a single battery for energy storage can lead to excessive capacity requirements, driving up investment costs. Additionally, frequent charging and discharging, along with a high depth of discharge (DOD), can significantly shorten the battery's cycle life and impair its normal operation. To address these issues, optimizing the configuration of energy storage systems (ESSs) to balance performance, cost, and longevity effectively is crucial.(2)

In recent years, ongoing research has been aimed at developing strategies for the optimal deployment of hybrid energy storage systems (HESSs) to achieve maximum efficiency and reliability.(3,4) Currently, numerous researchers are focused on the control strategies for HESSs to stabilize power source fluctuations and optimize the capacity configuration. Some achievements have contributed to enhancing the operational efficiency and reliability of HESSs in managing power output fluctuations.(5,6) For instance, the low-pass filtering principle has been employed to allocate energy storage power; however, it may lead to filtering delays if the time constant is not selected appropriately. Alternatively, the discrete Fourier transform (DFT) has been utilized to decompose unbalanced wind power, but it requires the presetting of basis functions, which increases the complexity of the optimization process.(7,8) Huang *et al.* introduced wavelet decomposition methods for HESS capacity configuration.(9) Yanan *et al.* first applied wavelet decomposition to determine the reference power for a HESS, followed by a secondary correction using a fuzzy controller to achieve a balanced power distribution within the HESS.(10) However, the results were very sensitive to the choice of wavelet bases. Also, wavelet decomposition is limited to processing linear nonstationary signals. Furthermore, empirical mode decomposition (EMD) combined with neural networks (NN) has been used to allocate HESS power, but EMD may suffer from mode mixing, affecting the accuracy of the energy storage configuration.

The anti-pulse interference average (AIAF) method was proposed to smooth the original wind power and then compensate for the low accuracy of EMD using DFT, ultimately allocating the energy storage capacity.(11) However, the AIAF may cause a certain delay during the process. A combination of moving average filtering (MAF) and EMD was suggested to maximize benefits for the energy storage capacity configuration. Poor suppression and filtering delays may occur because the MAF is ineffective for high-frequency signals. Variational mode decomposition (VMD) was reported to allocate the internal power of HESS. Although it can effectively solve the problem of modal aliasing, presetting of the modal order in the decomposed model was required.(12) Therefore, poor adaptability cannot be avoided. In complete ensemble empirical mode decomposition with adaptive noise (CEEMDAN), auxiliary Gaussian white noise was introduced to improve the signal decomposition accuracy, which reduced reconstruction errors. A CEEMDAN-based power allocation strategy was developed wherein mutual information entropy was employed to partition HESS power into distinct frequency bands.[13] However, it cannot intuitively indicate the occurrence of mode mixing between adjacent modal components.

To address the current research shortcoming, we propose a novel HESS architecture in which battery and supercapacitor technologies are combined to stabilize wind power. The framework utilizes *K*-means clustering of historical generation data to establish typical operation modes, with scenario selection optimized for maximum noise conditions through median-based fluctuation analysis. The MAF and AIAF weighted filtering algorithms were applied to obtain wind power, grid-tied power, and HESS reference power. The EEMD, CEEMDAN, and ICEEMDAN decomposition techniques were compared. Through ICEEMDAN and Hilbert transform processing, we systematically separate the HESS power requirements into high- and low-frequency elements for optimal storage allocation. The high-frequency component is allocated to the supercapacitor, while the low-frequency component is assigned to the storage battery. Actual data is used to demonstrate the effectiveness of the energy storage configuration.

2. Model of HESS Power Generation System

2.1 Fundamentals of wind and energy storage system

This study is focused on centralizing energy storage allocation at the point of interconnection between wind farms and the main power grid. Figure 1 shows the complete topological layout of the combined wind power and energy storage system. The selection of lead-acid batteries over lithium-ion batteries was driven by their cost-effectiveness, resulting in lower capital expenditure for the system. In this context, $P_{wind}(t)$ represents the initial output power, $P_{hess}(t)$ denotes the reference power of the HESS, $P_{bat}(t)$ represents the battery's reference power output, $P_{sc}(t)$ is the reference power of the supercapacitor, and $P_{grid}(t)$ refers to the reference power of the grid-tied wind system.

Equations (1) and (2) are derived from the power relationships shown in Fig. 1.

$$P_{grid}(t) = P_{wind}(t) + P_{hess}(t) \tag{1}$$

$$P_{hess}(t) = P_{bat}(t) + P_{sc}(t) \tag{2}$$

From Eq. (1), it is evident that the difference between the wind grid-connected reference power and the original wind output power constitutes the reference power of the HESS. When $P_{hess}(t) > 0$, the HESS discharges; in contrast, when $P_{hess}(t) \leq 0$, the HESS charges.

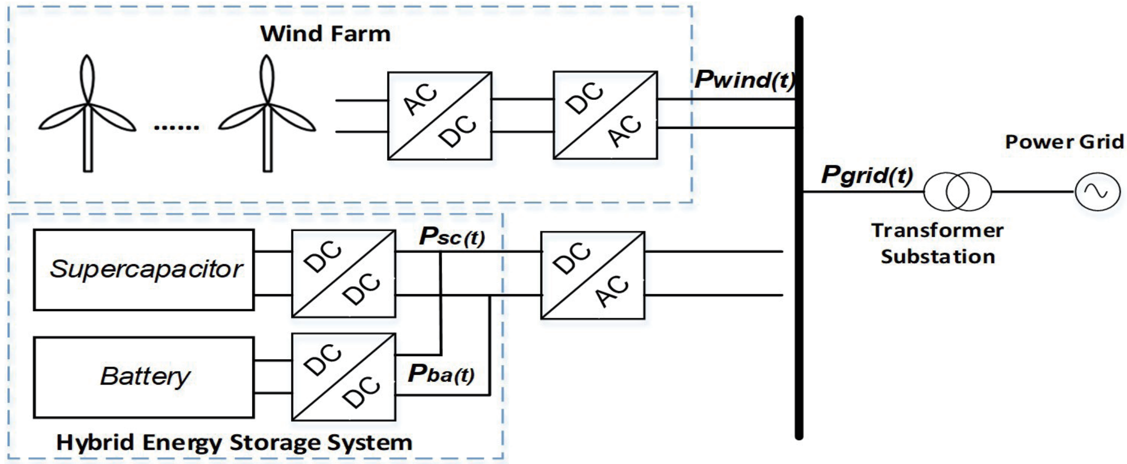

Fig. 1. (Color online) Diagram of wind and energy storage system structure.

2.2 Standards for wind power grid integration

According to wind power grid connection regulations around the world, wind farms must maintain stable output. For example, the grid-connected power with specific standards is defined for 10-min and 1-min intervals, as detailed in Table 1.[14] This ensures that active power variations remain within specified thresholds, thereby safeguarding the stability and reliability of the power system.

2.3 Scene selection based on *K*-means clustering algorithm

Developed by MacQueen (1967), the *K*-means algorithm is a foundational technique in unsupervised learning, renowned for its simplicity and effectiveness in clustering analysis. Its widespread adoption stems from its ability to efficiently partition datasets into a predetermined number of distinct clusters, each treated as an independent subgroup. This decomposition of complex data into simpler, homogeneous clusters not only enhances interpretability but also significantly reduces computational overhead. The algorithm's step-by-step procedure is systematically outlined in the flowchart presented in Fig. 2.

2.4 Typical days and data selection

The *K*-means clustering algorithm was implemented to analyze wind power data. To facilitate the smoothing of power fluctuations for typical days in subsequent studies, representative days were chosen by optimizing both the cluster centroid proximity and volatility levels. Here, fluctuations are quantified as the absolute differences between consecutive one-min power measurements, while cumulative daily fluctuations represent the aggregate sum of these variations. For each cluster, the sample exhibiting the median fluctuation value was designated as the typical day dataset. The typical day dataset with the highest noise level is selected for

Table 1
List of wind power grid integration standards in major countries.

Country	Wind power grid integration standards
United States	Maintain instantaneous ramp rates below 10% of total installed capacity per 1 min
Canada	Maintain instantaneous ramp rates below 10% of total installed capacity per 1 min
Denmark	Maintain instantaneous ramp rates below 5% of total installed capacity per 1 min
Germany	Maintain instantaneous ramp rates below 10% of total installed capacity per 1 min
United Kingdom	1-min power variation threshold: 10 MW & 1-min/10-min ramp rate ratio: ≤3:1
China	Installed capacity <30 MW: Maximum 10-min power deviation: 10 MW & Maximum 1-min power fluctuation: 3 MW
	Installed capacity 30–150 MW: Maximum 10-min output deviation: 33.3% of rated capacity & Maximum 1-min output change: 10% of nameplate capacity
	Installed capacity >150 MW: 10-min power fluctuations within 50 MW & 1-min power fluctuations below 15 MW

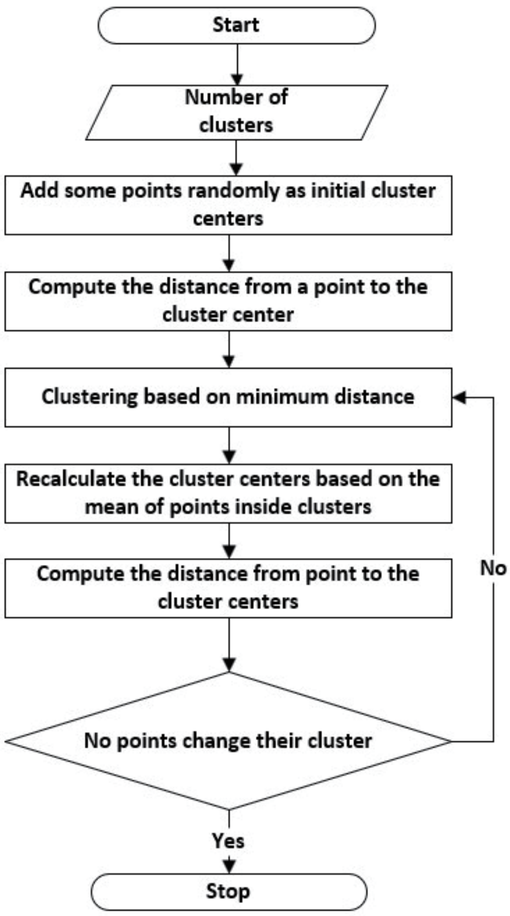

Fig. 2. Flowchart of *K*-means algorithm scene selection.

subsequent analysis. The block diagram illustrating the typical day and data selection methodology is shown in Fig 3.

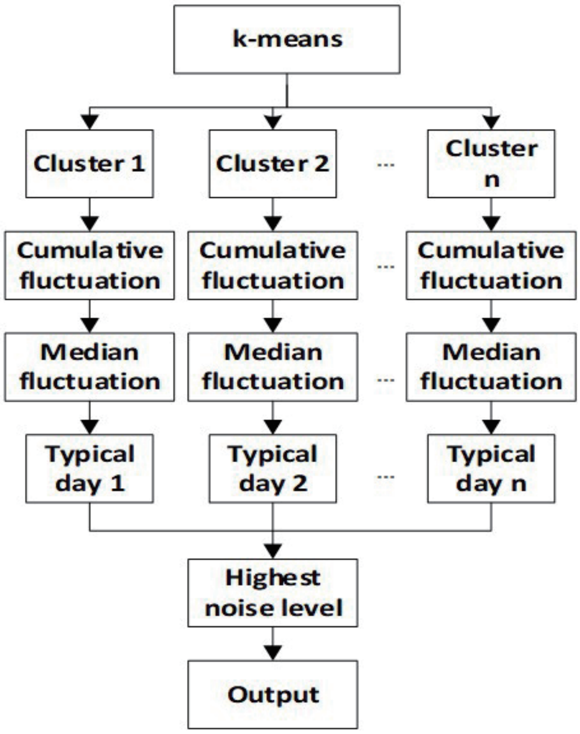

Fig. 3. Flowchart of typical day and data selection.

3. Wind power fluctuation suppression methods

The active power of the wind power station must meet the grid-tied requirements outlined in Sect. 2.2. Fluctuations across distinct time resolutions (1-min and 10-min intervals) are analyzed to assess both rapid variability and sustained deviations, with comparative results presented in Table 1. To achieve a smooth active power curve representing the grid-tied wind power, filtering is carried out. In this study, the raw wind output power is treated as a noisy signal to be filtered out.

3.1 MAF method

By the MAF technique, the mean of all values within a specified time window is calculated, progressing sequentially to produce the expected output as the window advances.[15] In the context of wind power output, the power data is sampled following the MAF principle. Each iteration forms a new data array of length by removing the oldest data point (first in, first out) and computing the arithmetic mean of the new array. Figure 4 shows the block diagram of MAF. This process is repeated to generate subsequent data arrays, ultimately yielding a highly smooth output for wind power generation.

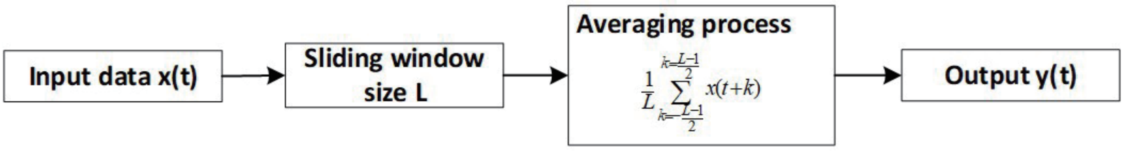

Fig. 4. MAF block diagram.

The grid-tied wind power $P_{sli}(t)$ used to smooth wind power output is expressed as

$$P_{sli}(t)=\frac{1}{L}\left[P_{wind}\left(t-\frac{L}{2+1}\right)+P_{wind}\left(t-\frac{L}{2+2}\right)+\ldots+P_{wind}\left(t\right)+\ldots+P_{wind}\left(t+\frac{L}{2}\right)\right], \quad (3)$$

where L is the moving filtering window, treated as an even number here.

3.2 AIAF method

The wind power output signal undergoes preprocessing by AIAF. It collects M data samples, eliminates outlier values (maximum and minimum), and computes the arithmetic average of the residual data points. The resultant data array is then produced, yielding a smooth output for wind power generation. The grid-tied wind power $P_{mid}(t)$ derived from AIAF for the suppression of wind output power is represented by

$$P_{mid}(t)=\frac{1}{M-2}\left[P_{wind}(t-M)+P_{wind}(t-M+1)+\ldots+P_{wind}(t)-P_{wind,max}-P_{wind,min}\right], \quad (4)$$

where $P_{mid}(t)$ denotes the grid-tied wind power derived using the AIAF technique. The variable M denotes the cardinality of the filtered data subset. $P_{wind,\,max}$ and $P_{wind,\,min}$ correspond to the maximum and minimum values within the M filtered dataset, respectively. The index t counts each wind power measurement $P_{wind}(t)$, with one sample recorded every minute.

3.3 Weighted filtering

While the aforementioned filtering methods can smooth the wind power output signal effectively, they still present certain issues. Selesnick and coworkers proposed a power fluctuation smoothing algorithm with a combination of low-pass filtering and least-squares fitting. It can mitigate the time delay problem of low-pass filtering and the smoothing limitations of least-squares fitting.[16] Hence, we combine the advantages of MAF and AIAF. The weights of these methods are dynamically adjusted on the basis of the degree of wind power fluctuation, as shown in

$$P_{wind,grid}(t)=(1-\theta)P_{mid}(t)+\theta P_{sli}(t), \quad (5)$$

where θ is the weight of the filtering model.

$$\theta = \begin{cases} 0, & \sigma \le h_1 \\ (\sigma - h_1) \times \mu / (h_2 - h_1), & h_1 < \sigma < h_2 \\ \mu, & \sigma \ge h_2 \end{cases} \tag{6}$$

Here, h_1 and h_2 are the maximum and minimum thresholds of the wind output standard deviation, respectively; $\mu \in (0,1)$. In Eq. (7), $\sigma(t)$ is the standard deviation of the wind power output. The greater the wind power fluctuation, the greater $\sigma(t)$ is, where n is the wind power dataset number. $\overline{P}_{wind}$ is the average value of the wind power output.

$$\sigma(t) = \sqrt{\frac{1}{n}\sum_{t=0}^{n}\left(P_{wind}(t) - \overline{P}_{wind}\right)^2} \tag{7}$$

When $\sigma \le h_1$ and $\theta = 0$, AIAF can meet the wind power fluctuation requirements. If the degree of fluctuation becomes increasingly severe, θ increases with the increase in σ. At this stage, incorporating a smoother MAF method is necessary to mitigate wind output fluctuations. When $\sigma \ge h_2$, the weight θ no longer changes, and its value is fixed as μ.

4. Decomposition process using modal analysis

Accurate real-time monitoring of wind power generation is critical for efficient energy storage management and signal analysis. Contemporary wind installations employ comprehensive sensor arrays featuring precision power measurement devices and advanced anemometry systems. The acquired data forms the basis for our fluctuation mitigation approach, undergoing initial weighted filtering before ICEEMDAN decomposition and Hilbert spectral analysis. The reliability of this control strategy is fundamentally dependent on the measurement accuracy and temporal resolution of the sensor infrastructure.

4.1 ICEEMDAN decomposition

EMD is a method particularly suitable for analyzing nonlinear data. Compared with traditional methods, EMD is more intuitive, direct, and adaptive.(17) A novel decomposition method combines ICEEMDAN and the Hilbert transform (HT), resulting in the enhanced ICEEMDAN-HT. The modified Hilbert envelope signal is subsequently combined with an enhanced residual network architecture through integration.

Building upon EEMD's limitations, Torres *et al.* developed CEEMDAN, which incorporates adaptive non-Gaussian white noise at each decomposition stage. This advanced technique generates both intrinsic mode functions (IMFs) and associated residual signals through its iterative process.(18) In EEMD, decomposing a signal containing noise can result in variations in the IMF components because of the different ways of adding noise. CEEMDAN effectively resolves this issue.

Two new operators are introduced: $M(\cdot)$ and $E_k(\cdot)$. $M(\cdot)$ represents the local mean value of the original signal obtained through EMD, while $E_k(\cdot)$ constructs the EMD decomposition model. Below is a step-by-step explanation of the ICEEMDAN decomposition process.

Step 1: Add Gaussian white noise to the original signal.

$$P_i = P + \beta_0 E_1\left(W_i\right) \tag{8}$$

P represents the input signal, β_0 denotes the standard deviation of injected Gaussian noise, W_i represents a zero-mean Gaussian white noise process with null variance, and $E_1(\cdot)$ is the operator extracting the first IMF.

Step 2: Determine the initial residual value:

$$r_1 = \frac{1}{N}\sum_{i=1}^{N} M\left(P_i\right), \tag{9}$$

where N denotes the number of data points in the original signal P.

Step 3: In the ICEEMDAN framework, each mode corresponds to a distinct frequency band, with $k = 1$ denoting the highest-frequency intrinsic mode function.

$$IMF_1 = \frac{1}{N}\sum_{i=1}^{N} E_1(P) = P - r_1 \tag{10}$$

Step 4: When k is set to 2, the second residual is obtained by calculating the local mean of r_1 after incorporating Gaussian white noise through the EMD process.

$$r_2 = \frac{1}{N}\sum_{i=1}^{N} M\left(r_1 + \beta_1 E_2\left(W_i\right)\right) \tag{11}$$

The second modal component is derived by calculating the difference between r_1 and r_2.

$$IMF_2 = r_1 - r_2 = r_1 - M\left(r_1 + \beta_1 E_2\left(W_i\right)\right) \tag{12}$$

Step 5: For decomposition levels $k = 3$ to K, the ICEEMDAN procedure computes both the k-th residual component r_k and the corresponding k-th intrinsic mode function IMF_k.

$$r_k = \frac{1}{N}\sum_{i=1}^{N} M\left(r_{k-1} + \beta_{k-1} E_k\left(W_i\right)\right) \tag{13}$$

$$IMF_k = r_{k-1} - r_k \tag{14}$$

Decomposition proceeds cyclically until the residual meets monotonicity criteria, at which point the original signal is resolved into a collection of oscillatory modes and a trend component.

$$P = r_n + \sum_{i=1}^{N} IMF_i \tag{15}$$

4.2 Extraction of instantaneous frequency from Modal function

The HT method is a highly effective approach for processing nonlinear signals. It not only facilitates the analysis of the signal's frequency domain characteristics but also enables the extraction of both the real and imaginary power spectra of the original signal.(19) To enhance the accuracy and optimize the capacity allocation, selecting an optimal frequency partitioning approach that capitalizes on ICEEMDAN's distinctive decomposition characteristics is crucial. The developed technique successfully minimizes mode mixing artifacts between adjacent instantaneous frequency components in joint time–frequency analyses. The power signal of HESS is represented as

$$P_{hess}(t) = \sum_{k=1}^{n} IMF_k(t) + r_n(t) = \sum_{k=1}^{n} e_k(t) + r_n(t). \tag{16}$$

For the modal component $IMF_i(t)$, the HT to obtain the corresponding $H[IMF_k(t)]$ is

$$H[IMF_k(t)] = \frac{1}{\pi}\int_{-\infty}^{+\infty} \frac{IMF_k(\tau)}{1-\tau} d\tau. \tag{17}$$

The corresponding analytical signal z(t) is constructed through the HT:

$$z_k(t) = IMF_k(t) + jH[IMF_k(t)] = \varphi_k(t)\exp[j\phi_k(t)], \tag{18}$$

$$\varphi_k(t) = \sqrt{IMF_k^2(t) + H^2[IMF_k(t)]}, \tag{19}$$

$$\phi_k(t) = \arctan\frac{H[IMF_k(t)]}{IMF_k(t)}, \tag{20}$$

$$\omega_k(t) = \frac{d\phi_k(t)}{dt}. \tag{21}$$

In Eq. (19), $\varphi_k(t)$ denotes the instantaneous amplitude envelope of each IMF and $\phi_k(t)$ represents the instantaneous value of each IMF phase. $\omega_k(t)$ represents the instantaneous value of each IMF frequency, and finally, the Hilbert time–frequency spectrum $H(\omega,t)$ expressed in polar coordinates is obtained. The analysis of the time–frequency spectrum reveals the temporal evolution and spectral characteristics of the power signal across all frequency bands. The specific law is shown as

$$H(\omega,t)=\mathrm{Re}\left\{\sum_{k=1}^{n}\phi_k(t)\exp\left[j\int\omega k(t)dt\right]\right\}. \tag{22}$$

4.3 Internal power distribution control strategy for batteries and supercapacitors

Through the analysis presented in Sect. 5.2, the process of extracting instantaneous frequency characteristics of IMFs by the ICEEMDAN-HT method is illustrated in Fig. 5. Initially, the instantaneous frequency–time curves IMF1 to IMFk are derived, ranging from high- to low-frequency bands. Subsequently, the curves IMFm and IMFm+1, which have no or minimal modal mixing, are selected from these curves. The curve IMFm and the modal components with instantaneous frequencies higher than IMFm are then accumulated and reconstructed to be absorbed by the supercapacitor. Meanwhile, IMFm+1 and the modal components with instantaneous frequencies lower than IMFm+1 are accumulated to be absorbed by the battery. Consequently, the result of power allocation for the HESS is determined to be

$$\begin{cases} P_{sc}(t)=\sum_{k=1}^{m}IMF_k(t), \\ P_{bat}(t)=\sum_{k=m+1}^{n}IMFk(t)+r_n(t), \end{cases} \tag{23}$$

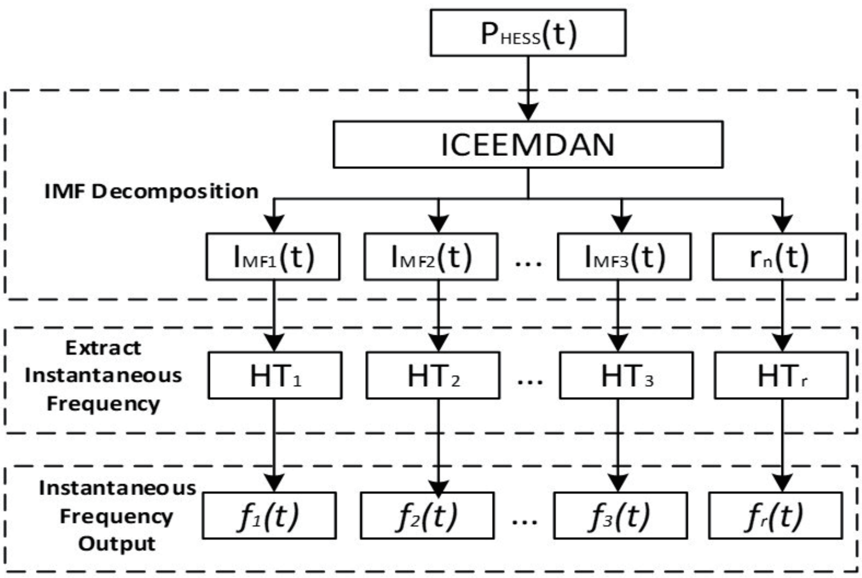

Fig. 5. Process of ICEEMDAN-HT extraction of IMF instantaneous frequency.

where $P_{sc}(t)$ is the reconstructed supercapacitor reference power, $P_{bat}(t)$ is the reconstructed battery reference power, and $r_n(t)$ is the residual. The strategy of power allocation for HESS described in Sects. 2.2–2.7 is illustrated in Fig. 6.

5. Simulation Results and Discussion

5.1 Clustering in generating typical day

The *K*-means clustering algorithm was applied to 1-min wind power data from a 2 MW system over an entire year. The total number of days, probability, fluctuation, and noise levels for different cluster configurations are presented in Table 2. Table 2 presents the results of a statistical analysis of four clusters for various parameters. The "Total Days" row quantifies the number of days each cluster was observed, with Cluster Three exhibiting the highest count (134 days) and Cluster One the lowest (49 days).

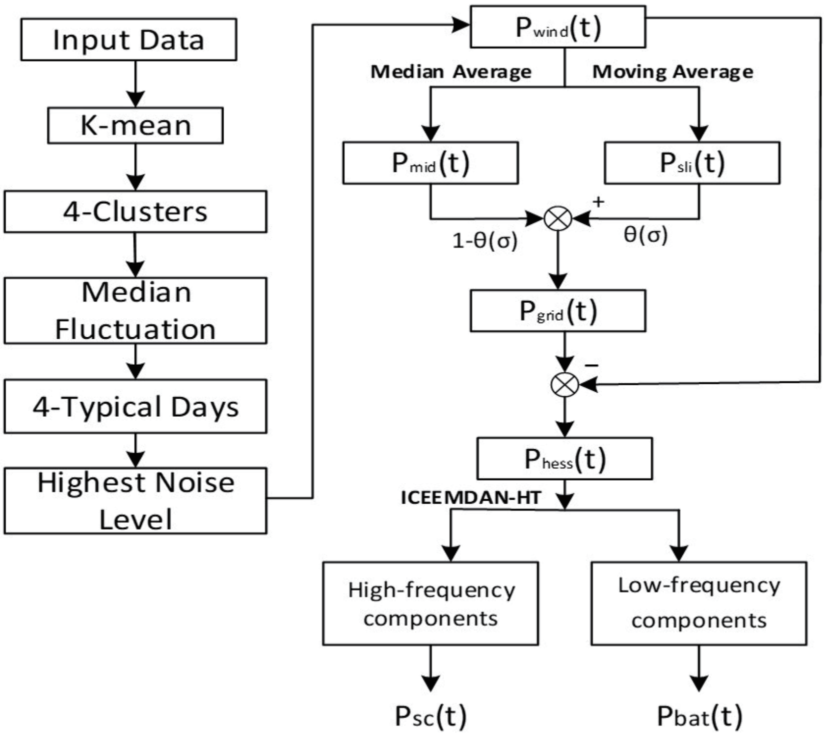

Fig. 6. Power allocation strategy for HESS.

Table 2
Results of a statistical analysis of four clusters.

Cluster	One	Two	Three	Four
Total days	49	71	134	111
Total days probability (%)	13.42	19.45	36.71	30.41
Median fluctuation	42	17	67	63
	Typical Day 1	Typical Day 2	Typical Day 3	Typical Day 4
Highest noise level	0.5676	0.62228	0.19159	0.2503

"Total Days Probability" represents the proportion of each cluster within the dataset, where Cluster Three accounts for the largest percentage (36.71%). "Median Fluctuation" shows the median fluctuation values across clusters, which are used to identify a typical day within each cluster on the basis of the median fluctuation value. Finally, "Highest Noise Level" indicates the maximum noise levels recorded on the selected typical day for each cluster, with Cluster Two demonstrating the highest noise level (0.62228). For further analysis, the typical day from Cluster Two is selected.

The clustering analysis results visualized in Fig. 7 demonstrate the grouping of daily wind generation patterns, with each cluster's member profiles depicted in unique colors. Cluster 1 exhibits stable power generation with a clear diurnal pattern, indicating consistent wind speeds and reliable power production. Cluster 2, however, shows highly irregular generation with abrupt fluctuations, suggesting unstable wind conditions and inefficient power output. Cluster 3, with the highest number of days, experiences significant turbulence, leading to chaotic power fluctuations and challenges in maintaining a steady grid supply. Cluster 4 demonstrates moderate variability, with noticeable but more structured fluctuations than Cluster 3. While not as stable as Cluster 1, power output is more manageable than the turbulence of Cluster 3. The characteristic wind generation patterns for all four clusters are presented Fig. 8.

5.2 Suppression of wind power fluctuation

The MAF method and weighted filter method are employed to smooth the wind power output. With the window parameters set to $L = M = 20$, the impact of the MAF method on reducing wind power fluctuations is depicted in Fig. 9. The original wind power output curve presents a smoother trend, with significantly diminished random fluctuations. Figure 10 illustrates that the signal remains unsmoothed at higher frequencies because of the low-pass-

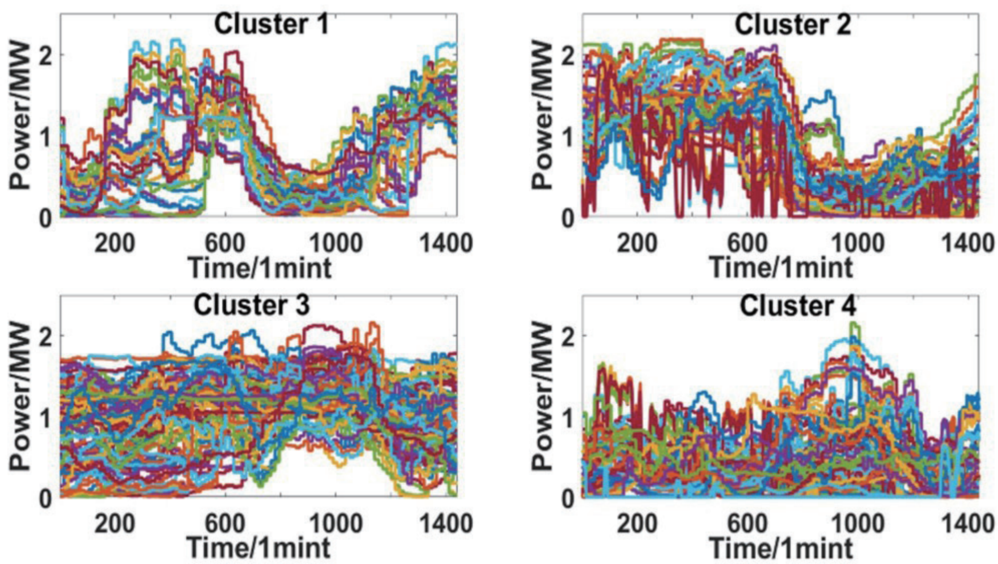

Fig. 7. (Color online) Results of *K*-means clustering.

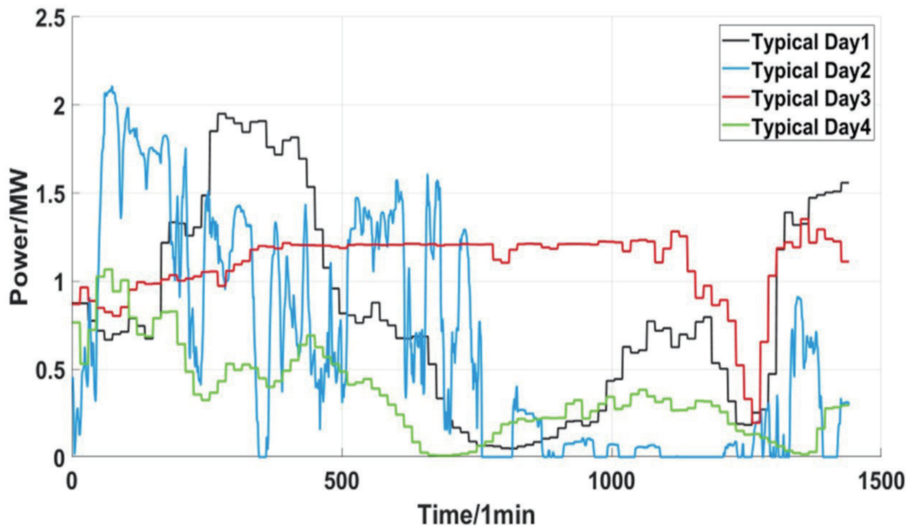

Fig. 8. (Color online) Typical daily wind power curves.

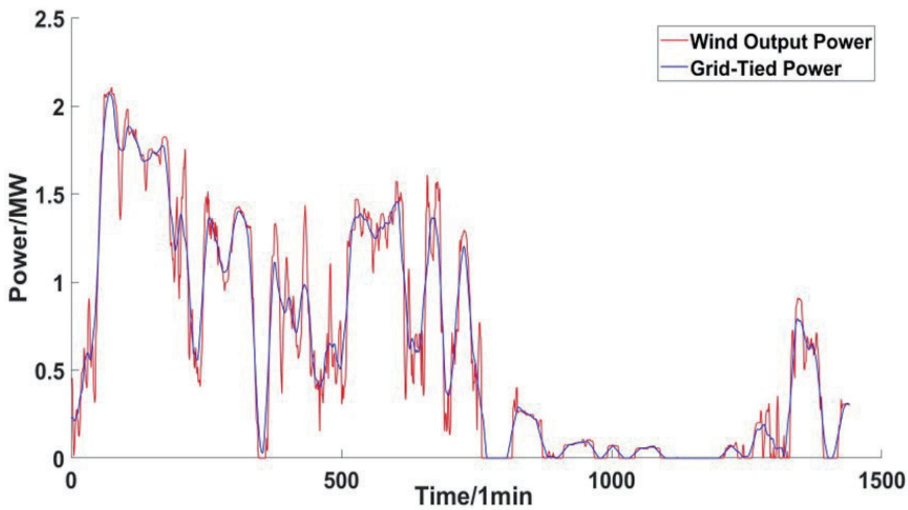

Fig. 9. (Color online) Effect of stabilizing wind power fluctuations by moving average.

filter nature of the MAF method and its inherent delay issue. The effect of suppressing wind power fluctuations by the weighted filtering method is illustrated in Fig. 8. It is evident that the grid-tied wind power, after being processed by weighted filtering, closely aligns with the original output power, resulting in a signal that is smoothed even at higher frequencies. This is particularly noticeable in the figures where abrupt changes in the output power are mitigated.

As observed in Fig. 9, there is no time delay, and the original wind power output is 0.697 MW at approximately 00:46 mins. After applying MAF, the grid-connected wind power increases to 0.885 MW, requiring the HESS to release 0.188 MW to smooth power fluctuations. Following weighted filtering, the grid-connected power is reduced to 0.727 MW, significantly lowering the

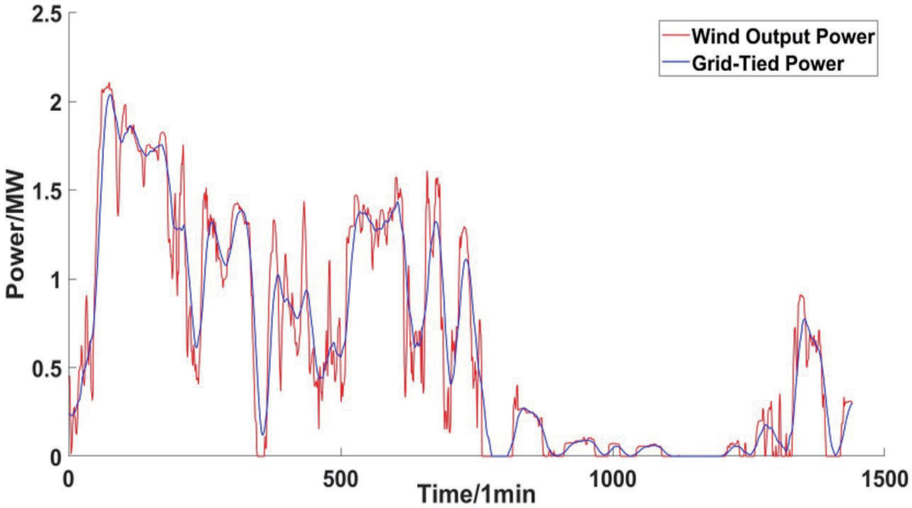

Fig. 10. (Color online) Effect of stabilizing wind power fluctuations by weighted filtering.

required energy release to 0.03 MW. The proposed weighted filtering method reduces the energy storage demand by approximately 0.185 MW, minimizing unnecessary output. Experimental results indicate this methodology not only decreases capital expenditures but also extends the operational lifespan by optimizing component utilization.

In Table 3, the maximum wind power fluctuations obtained with the MAF method within 1 min and 10 min are 0.0866 and 0.6769 MW, respectively, both of which comply with grid-tied requirements. On the other hand, the maximum wind power fluctuations when using the weighted filtering method within 1 min and 10 min are 0.0667 and 0.5962 MW, respectively, both meeting grid-tied requirements. Although both methods can effectively suppresses wind power fluctuations, the weighted filtering method presents a slightly better performance than the MAF method.

5.3 Analysis of HESS power decomposition and frequency domain

Following the acquisition of the reference grid-connected wind power, the HESS reference power is computed as the difference between this reference and the original wind output. Figure 11 shows that the HESS operational behavior exhibits nonstationary and nonlinear power exchange dynamics. The HESS reference power is decomposed using ICEEMDAN with a noise ratio of 0.1, 100 noise additions, and 5000 iterations. Figure 12(a) shows nine IMFs in descending frequency and a residual, while Fig. 12(b) presents their spectra obtained via fast Fourier transform. The HESS power is divided into ten frequency bands from 0 to 0.5 Hz.

To highlight the advantages of ICEEMDAN over EEMD and CEEMDAN in the HESS configuration, EEMD is used to decompose the reference power. Figure 13 shows modal aliasing between adjacent components, making frequency separation challenging. Figure 14 shows that CEEMDAN reduces aliasing between IMFs 10 and 11 compared with EEMD, but some aliasing remains, affecting the battery cycle life. ICEEMDAN decomposition is presented in Fig. 15; it

Table 3
Power fluctuation using various methods.

Period of time	Power fluctuation status	Original	MAF method	Weighted filtering method
1 min	Maximum power fluctuations (MW)	0.5165	0.0866	0.0667
	Maximum grid-connected power fluctuation rate (%)	84.1654	14.1125	10.8724
10 min	Maximum power fluctuations (MW)	1.3250	0.6769	0.5962
	Maximum grid-connected power fluctuation rate (%)	215.9034	110.3111	97.1605
	Smoothness index (%)	0.9121	0.0042	0.0022

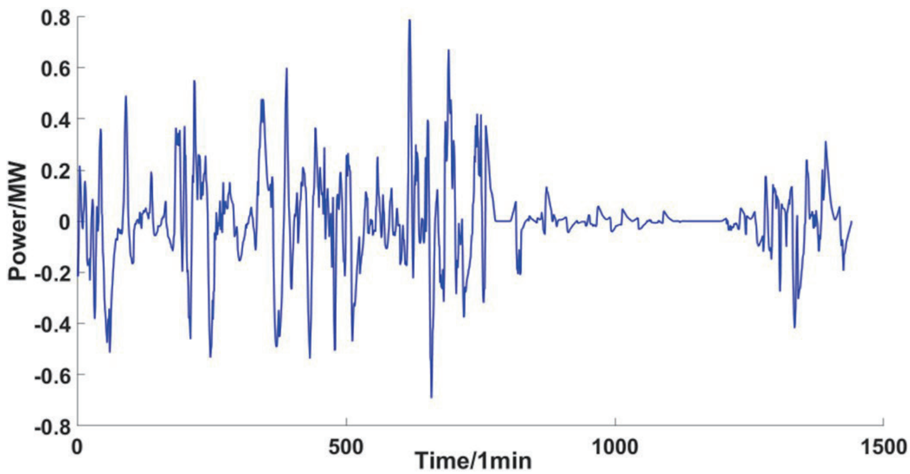

Fig. 11. (Color online) Operating status of HESS.

yields nine IMFs and one residual. Unlike previous methods, IMFs 8 and 9 exhibit minimal aliasing, allowing for clear separation. IMF8 and higher-frequency components are assigned to the supercapacitor, while IMF9 and the residual are allocated to the battery.

Figure 13 shows that IMF6 approaches zero, revealing a fundamental EEMD limitation due to its noise-assisted decomposition structure. This oscillatory loss stems from incomplete mode alignment and will affect the reconstruction precision. CEEMDAN and ICEEMDAN overcome these limitations through the use of improved decomposition algorithms.

Table 4 presents the results of a comparative analysis of EEMD, CEEMDAN, and ICEEMDAN based on key performance metrics. Among these algorithms, ICEEMDAN attains the lowest *OI* (0.80074), indicating better mode separation. It also exhibits the highest *ER* (0.92818), suggesting superior energy preservation. Additionally, it significantly presents the lowest *MSE* (6.0789×10^{-34}) and achieves the highest *SNR* (316.59).

Figures 16 and 17 present the outcomes of applying the operational strategy of the hybrid energy storage system (HESS) through ICEEMDAN-based component allocation. Figure 16 shows the decomposition results, where high-frequency intrinsic mode functions (IMFs 1–8) are

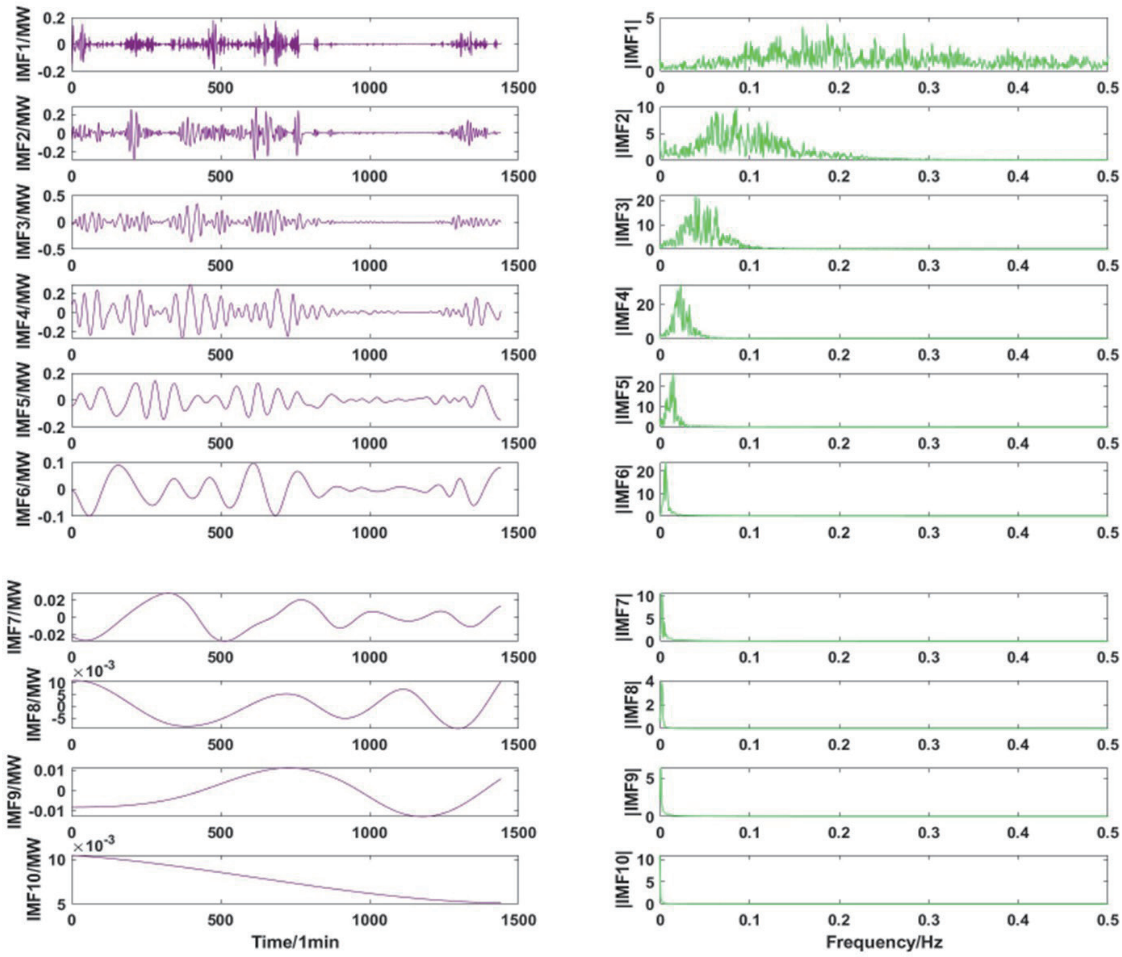

(a) (b)

Fig. 12. (Color online) IMF components obtained by ICEEEMDAN decomposition and spectrograms.

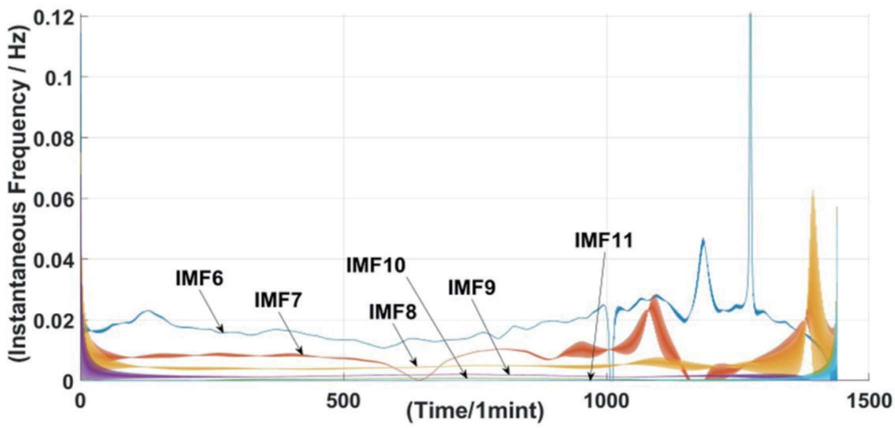

Fig. 13. (Color online) Instantaneous frequency–time curves of EEMD's IMF.

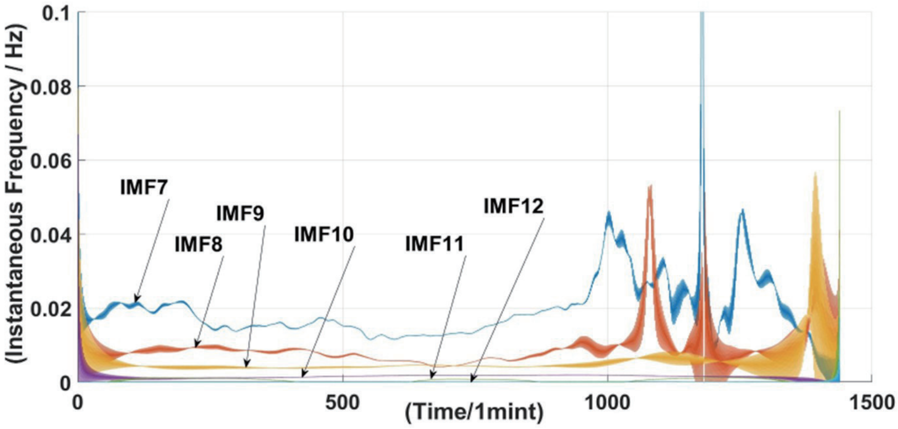

Fig. 14. (Color online) Instantaneous frequency–time curves of CEEMDAN's IMF.

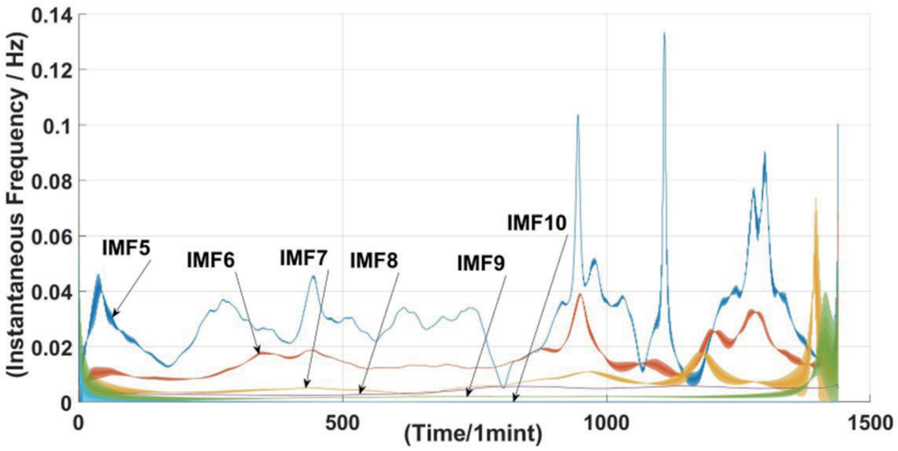

Fig. 15. (Color online) Instantaneous frequency–time curve of ICEEMDAN's IMF.

assigned to supercapacitors to capitalize on their fast dynamic response characteristics. Figure 17 shows the corresponding allocation of low-frequency components (IMF 9 to residual) to the battery bank, utilizing its superior energy storage capacity for sustained power delivery. In contrast, batteries operate over longer cycles with smoother charging and discharging, making them suitable for sustained energy supply. HESS significantly reduces the battery workload, enhancing its lifespan and mitigating thermal issues caused by excessive charge–discharge cycles. By reducing thermal runaway risks and exothermic reactions, HESS improves battery safety and the overall system reliability.

Table 4
Results of comparative analysis of various methods.

Parameters	EEMD	CEEMDAN	ICEEMDAN
Orthogonality index (*OI*)	1.4494	1.3389	0.80074
Energy ratio (*ER*)	0.67006	0.71756	0.92818
Mean squared error (*MSE*)	2.4567×10^{-6}	1.03×10^{-33}	6.0789×10^{-34}
Signal-to-noise ratio (*SNR*)	40.524	314.3	316.59

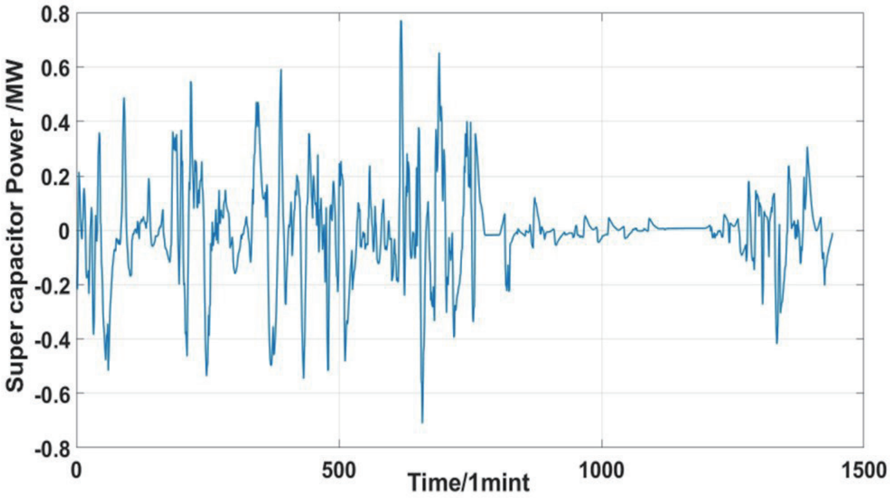

Fig. 16. (Color online) Supercapacitor reference power.

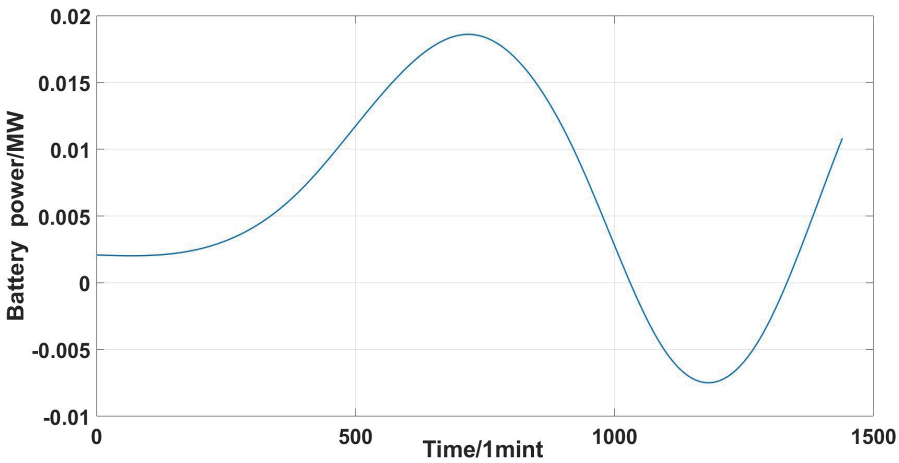

Fig. 17. (Color online) Battery reference power.

6. Conclusions

We demonstrated an effective approach for smoothing wind power fluctuations through a HESS. From actual wind output data, *K*-means clustering was employed to extract representative daily data, followed by weighted filtering to smooth fluctuations while preserving the original power profile with minimal time delay. This is superior in decreasing the configuration capacity of the energy storage system—resulting in cost savings—as well as in enhancing its energy utilization efficiency, mitigating risks associated with power fluctuations. The grid-tied reference power was further decomposed using ICEEMDAN, and the instantaneous frequency–time curves obtained via HT provided insights into mode correlations. A comparative analysis of EEMD, CEEMDAN, and ICEEMDAN confirmed that ICEEMDAN effectively separates high-frequency and low-frequency components, enabling a more optimal energy storage configuration. For example, ICEEMDAN attains the lowest *OI* and the highest *ER*. Moreover, it achieves the lowest *MSE* with the highest *SNR*. Furthermore, HESS can significantly improve the battery workload so that thermal issues are effectively mitigated. In conclusion, valuable guidance for designing HESSs can be offered for wind power stations, enhancing system stability and efficiency.

Acknowledgments

This study was supported by Science and Technology Program of Chengde City, People's Republic of China (Project No. 202305B029) and Tianjin Carbon Peak and Carbon Neutrality Technology Major Project (Grant no. 24ZXTKSN00030) and Tianjin Natural Science Foundation Project (Grant no. 23JCQNJC01060)."

References

1 S. Roga, S. Bardhan, Y. Kumar, and S. K. Dubey: Sustain. Energy Technol. Assess. **52** (2022) 102239. https://doi.org/10.1016/j.seta.2022.102239
2 X. Zhang, L. Kang, X. Wang, Y. Liu, and S. Huang: Energies **18** (2025) 795. https://doi.org/10.3390/en18040795
3 Q. Fu, B. Jing, P. He, S. Si, and Y. Wang: IEEE Sens. J. **18** (2019) 5024. https://doi.org/10.1109/JSEN.2018.2830109
4 R. Hou, J. Liu, W. Chen, and J. Liu: J. Energy Storage. **111** (2025) 115392. https://doi.org/10.1016/j.est.2025.115392
5 S. Lei, Y. He, J. Zhang, and K. Deng: Energies **16** (2023) 11. https://doi.org/10.3390/en16114307
6 H. Han and Z. Tang: Power Syst. Prot. Control. **12** (2020) 90. https://doi.org/10.19783/j.cnki.pspc.190923
7 H. Li, X. Zhang, C. Xu, and J. Hong: IEEE Trans. Energy Convers. **35** (2019) 43. https://doi.org/10.1109/TEC.2019.2946888
8 L. Lin, L. Zhu, R. Yang, Y. Gao, and Q. Wu: 2017 2nd Int. Conf. Power and Renewable Energy (ICPRE, 2017) 61–65. https://doi.org/10.1109/ICPRE.2017.8390501
9 L. Huang, X. Zhang, S. Liang, R. Shi, S. Liao, and G. Zhang: Sci. Technol. Eng. **23** (2023) 10825.
10 Y. Li, Q. Wang, W. Song, and X. Wang: Power Syst. Prot. Control. **47** (2019) 58.
11 M. Khalid: Energies **12** (2019) 4559. https://doi.org/10.3390/en12234559
12 Y. Zhang and F. Zhao: J. Phys.: 2022 Conf. Ser., 2378. 1. 012048. https://doi.org/10.1088/1742-6596/2378/1/012048
13 Q. Li, G. Wang, X. Wu, Z. Gao, and B. Dan: Energy **299** (2024) 131448. https://doi.org/10.1016/j.energy.2024.131448

14 T. Sathiyanarayanan and Deepu Vijay M.: Power Systems Operation with 100% Renewable Energy Sources, S. Chenniappan, S. Padmanaban, and S. Palanisamy, Eds. (Elsevier, 2023) pp. 55–64. https://doi.org/10.1016/B978-0-443-15578-9.00007-8
15 C. Sun, Y. Yuan, S. Choi, M. S. Li, X. Zhang, and Y. Cao: Autom. Electr. Power Syst. **39** (2015) 19. https://doi.org/10.7500/AEPS20140719002
16 I. W. Selesnick, H. L. Graber, D. S. Pfeil, and R. L. Arbour: IEEE Trans. Signal Process. **62** (2014) 1109. https://doi.org/10.1109/TSP.2014.2298836
17 J. Y. Wu, S. Lan, S.-J. Xiao, and Y. B. Yuan: IEEE Access **9** (2021) 42226. https://doi.org/10.1109/ACCESS.2021.3062703
18 M. E. Torres, M. A. Colominas, G. Schlotthauer, and P. Flandrin: 2011 IEEE Int. Conf. Acoustics, Speech and Signal Processing (ICASSP, 2011) 4144–4147. https://doi.org/10.1109/ICASSP.2011.5947265
19 S. Bernstein: Adv. Appl. Clifford Algebras. **24** (2014) 921. https://doi.org/10.1007/s00006-014-0489-6

About the Authors

Muhammad Nouman Shahzad is a Ph.D. student in the electrical engineering department of Hebei University of Technology. He received his B.S. degree in electronic engineering from the International Islamic University, Islamabad, Pakistan and M.S. degree in electrical engineering from North China Electric Power University, Beijing, China. His research interests include hybrid energy storage systems, renewable energy grid integration, and control algorithms. (noumanshahzad45@gmail.com)

Obaid ur Rahman received his bachelor's degree in the field of electronics from the University of Swat, KPK, Pakistan, in 2021. He is currently pursuing his master's degree in electrical engineering at Hebei University of Technology, Tianjin, China. His research interest focuses on renewable energy, particularly solar energy, wind energy, and battery storage systems.
(Coax1432@gmail.com)

Hsiung-Cheng Lin graduated with a bachelor's degree in 1986 from National Taiwan Normal University, Taiwan. He received his master's and Ph.D. degrees from Swinburne University of Technology, Australia, in 1995 and 2002, respectively. From 2011 to 2019, he was a recipient of a special talent reward from the National Science Council, Taiwan. He is currently a full professor in the Department of Electronic Engineering at National Chin-Yi University of Technology. (hclin@ncut.edu.tw)

Asif Hussain received his M.phil. degree in physics from GC University Lahore, Pakistan, in 2006, M.Phil degree in microelectronics engineering and semiconductor physics from the University of the Punjab, Lahore Pakistan in 2013, and his Ph.D. degree in sustainable energy materials from Yangzhou University, China in 2023. Currently, he is an assistant professor in the Department of Physics, The University of Lahore, Pakistan. He is also handling editor of the International Journal of Physics and Materials Sciences. Currently, he is working on renewable energy materials.
(asif.hussain@phys.uol.edu.pk)

Ling-ling Li received her M.S. degree in control theory and control engineering in 2001 and her Ph.D. degree in electrical machinery and appliances in 2004 from Hebei University of Technology. She is currently a professor at the School of Electrical Engineering, Hebei University of Technology, and a permanent member of the State Key Laboratory of Reliability and Intelligence of Electrical Equipment. Her research interests include power systems, new energy, and electrical reliability.
(lilingling@hebut.edu.cn)